Neuro-Oncology Advances

8(1), vdaf251, 2026 | https://doi.org/10.1093/noajnl/vdaf251 | Advance Access publication December 8, 2025

A Cre-mediated copy number variant compromises the reliability of a *LoxP-STOP-LoxP-PLAG1* driven brain tumor model

Jan Vaillant, Sangita Pal, Jan Müller, Andrea Wittmann, Akosua Boakye-Yiadom, Philipp Sievers, Paula Zimmer, Melanie Schoof, Franziska Schelb, Nina Hofmann, Michaela-Kristina Keck, Tessa Fabian, Ulrich Schüller, Marc Zuckermann, Rameen Beroukhim, Pratiti Bandopadhayay, David T. W. Jones†, and Lena M. Kutscher†

All author affiliations are listed at the end of the article

Corresponding Authors: Lena M. Kutscher, German Cancer Research Center (DKFZ)/Hopp Children's Cancer Center (KiTZ), Im Neuenheimer Feld 280, 69120 Heidelberg, Germany (l.kutscher@kitz-heidelberg.de); David T. W. Jones, German Cancer Research Center (DKFZ)/Hopp Children's Cancer Center (KiTZ), Im Neuenheimer Feld 280, 69120 Heidelberg, Germany (david.jones@kitz-heidelberg.de).

†These authors jointly supervised this study.

Abstract

Background. The developmental context in which genetic alterations occur is crucial to understand disease progression. In pediatric cancer, modeling tumor formation in the right cell type is necessary to faithfully recapitulate the unique nature of pediatric tumors. The Cre-LoxP system is a powerful tool to modulate gene expression in specific cell types at discrete developmental time windows.

Methods. We used Cre-LoxP mouse models to study the role of the oncofetal transcription factor *PLAG1* in pediatric brain tumor formation. We characterized our model using histology, DNA methylation based copy number variant (CNV) analysis on fresh frozen and FFPE derived samples, RNA sequencing, whole genome sequencing and whole genome CRISPR Cas9 screening.

Results. We generated a new model for *PLAG1* overexpressing brain tumors, but discovered an unexpected CNV at the *Nras* locus by DNA methylation analysis. We confirmed the CNV via whole genome sequencing and found that it was likely mediated by Cre-recombination at the transgene insertion site. Both the tumor transcriptome and genetic dependencies are substantially shaped by this CNV.

Conclusions. Our work demonstrates the necessity of copy-number analysis when working with transgenic Cre-LoxP mouse models. Assessing CNVs should become a standard evaluation procedure when reporting new tumor models, preventing misleading conclusions that could dramatically impact the reliability of preclinical studies.

Key Points

- CNVs can arise in preclinical models in the presence of strong oncogenic drivers
- These alterations can then have a major impact on the model's dependencies
- DNA methylation array is a useful and cost-effective technique to determine CNVs

Received September 3, 2025; accepted December 2, 2025.

Importance of the study

Faithful animal models are an important tool for preclinical testing of ideas, molecules, and drugs for treatment of brain tumors. Our study demonstrates that DNA copy-number alterations by DNA methylation array should be assessed for every preclinical animal model, even in the presence of strong oncogenic drivers. We show that unintended copy-number changes can have a major influence on the dependencies of the model, which may affect downstream preclinical testing.

Basic and translational research relies on animal models, as current *in vitro* systems fail to capture the vast diversity of cell types present at the organismal level, including immune cells or transient cell states present during development.[1,2] Animal models are also indispensable for assessing drug responses or discerning toxicity preclinically.[3,4] Mice that have been genetically engineered to aberrantly express genes of interest, so called transgenic mice, are vital tools for cancer research. They allow the study of the functional consequences of disease- or cancer-related genes. One advantage is that tumors emerge *de novo,* in parallel to normal development, within an intact immune and microenvironmental context.[5] The Cre-LoxP system has been developed as a powerful tool to selectively activate transgenes in a lineage-specific manner.[6-8]These models are particularly useful for pediatric cancer research, as the developmental context of neoplastic transformation is important to faithfully recapitulate the biology of childhood cancers.[9] However, Cre-mediated artifacts have been described, including toxicity, leaky Cre expression, or germline recombination,[10-12] underlining the importance of careful characterization of Cre-LoxP mouse models before preclinical use.

The zinc-finger transcription factor *PLAG1* has been described as the driver oncogene in pleomorphic adenomas of the salivary gland, and it was shown that transgenic *LoxP-STOP-LoxP-PLAG1* (*LSL-PLAG1*) mice form pleomorphic adenomas upon crossbreeding to salivary-gland specific Cre-driver lines.[13,14] Additional solid tumors with aberrant *PLAG1* expression have since been described, including uterine leiomyosarcoma, lipoblastoma, rhabdomyosarcoma and fibromyxoid tumors.[15-18] Members of the *PLAG*-gene family are also found aberrantly activated in pediatric brain tumors. Central nervous system (CNS) embryonal tumors with PLAG family gene alteration (ET, PLAG) include *PLAG1*-fused tumors[19] or *PLAGL1/PLAGL2* amplified tumors,[20] while *PLAGL1*-fusions define a group of supratentorial neuroepithelial tumors (NET_PLAGL1)[21]; *PLAG1* is also highly expressed in diffuse midline gliomas and posteria fossa A ependymomas.[22] Altogether, this data suggests a broader role for the *PLAG* family in brain tumor development. Interestingly, *PLAG1* and its family members are usually expressed in the brain during fetal development.[23]We therefore hypothesized that aberrant overexpression of the oncofetal transcription factor *PLAG1* in the developing brain may lead to pediatric brain tumors, and such a model would have high preclinical value for several rare tumor entities.

To test this hypothesis, we used the previously described *LSL-PLAG1* mouse strain[14] and crossed it to CNS-specific *GFAP*-Cre and *Nes*-Cre driver mouse lines[7,8] with floxed *Trp53* knock-out alleles.[24] We found that brain tumors only emerged in the presence of *Trp53* inactivation. To our surprise, all derived tumors displayed a concurrent copy number gain on chromosome 3, encompassing a 10 Mb region surrounding the *Nras* locus. We show that this copy number gain significantly shapes the transcriptome and genetic dependencies of the tumor model. Our findings indicate that improper Cre-recombination at LoxP sites can lead to this copy-number alteration, compromising the reliability of this and similar models.

Methods

Animals

Lineage-specific *PLAG1*-overexpressing mice were generated by breeding *LSL-PLAG1R/LSL-PLAG1R* mice[14] with *hGFAP-Cre/+* mice[7] or with *Nes-Cre/+* mice[8], with or without floxed *Trp53* alleles.[24] Primer sequences for genotyping are shown in Supplemental Table 1. Animals were housed in a temperature-controlled facility with 12 h: 12 h light: dark cycle and *ad libitum* food and water in individually ventilated cages. All animals were inspected daily, and both sexes were used as experimental animals. When *hGFAP-Cre^{+}; LSL-PLAG1^{+}* animals showed first signs of abdominal tumor formation, no further breedings were initiated. All animal experiments for this study were conducted according to the animal welfare regulations approved by the responsible authorities (Regierungspraesidium Karlsruhe, approval number: G-35/20).

Hematoxylin and Eosin Staining

Brain or tumor samples were fixed in 10% formalin, dehydrated and embedded in paraffin and sectioned using a microtome. 5 µm sections were mounted on glass slides and deparaffinized for 10 min in 100% xylene. Following rehydration by immersion in descending ethanol solution (100%, 90%, 70%), slides were washed in distilled water. After application of hematoxylin on the slides for 5 min, samples were rinsed with tap water for 5 min. Eosin was applied for 3 min. The slides were washed in water for 20 s, followed by immersion in ascending ethanol solution. After a final immersion in xylene, slides were covered with a coverslip using mounting medium. Images were taken using the Zeiss Axioscan 7 (full-brain scans) or the Zeiss Cell Observer.

Immunohistochemistry

After deparaffinization and rehydration, 5 µm formalin-fixed paraffin-embedded (FFPE) sections were boiled in citrate buffer (citric acid 0.0018 M, sodium citrate 0.0082 M) for 20 min. The samples were allowed to cool to room temperature for 20 min, after this the sections were blocked with 10% normal donkey serum (NDS) in PBST for 1 h. Primary antibody in 10% NDS was applied to the section and incubated overnight at 4°C (Supplemental Table 2). The next day, slides were washed 3x for 10 min in PBST. The biotin-coupled secondary antibody (AffiniPure® Donkey Anti-Rabbit IgG, #711-065-152) in 10% NDS was applied and incubated for 1h at RT. Slides were washed 3× for 10 min in PBST and Vectastain® ABC-HRP was added to the slides for 30 min followed by a final wash step. DAB chromogen (Enzo Life Sciences #ACC-1050200) was applied for up to 5 min. The reaction was stopped by washing the slides in tap water. A 1:10 dilution of hematoxylin was applied to the sections for 1 min, followed by immersion of the slides in tap water for 5 min. Slides were dehydrated in ascending ethanol solution. After a final immersion in xylene, sections were mounted with coverslips. Stainings were quantified by analysing three regions of interest (50×50 µm) of three individual tumors with at least 200 nuclei. For nuclear markers, the proportion of positive nuclei was calculated. For non-nuclear markers, the proportion of positive stained area was calculated using ImageJ.

RNA Extraction, Sequencing and Analysis

Tumor tissue was homogenized (Tissue master, Omni Inc) and RNA was subsequently extracted using the Maxwell® RSC simplyRNA Tissue Kit. RNA quantity and integrity were assessed using the Agilent Bioanalyzer. 100 bp paired-end sequencing was performed on the NovaSeq 6000 (Illumina). Counts were analyzed using DeSeq2.[25,26] Volcano plots were generated using the R package EnhancedVolcano.

Generation of Cell Lines from Primary Tumors

Freshly-dissected tumor tissue was placed in pre-warmed TSM medium (Neurobasal-A and DMEM/F12 1:1 (Gibco™) with MEM Sodium Pyruvate Solution, MEM Non-Essential Amino Acids, GlutaMAX, Penicillin-Streptomycin (Gibco™, each 1× final concentration), HEPES (Gibco™, 0.01 M) and 20 ng/µL EGF, 20 ng/µL FGF, 10 ng/µL PDGF-A (Peprotech®). Tissue was homogenized by pipetting up and down multiple times. Large clumps were removed by filtering through a 45 µm cell strainer. The suspension was centrifuged, and the tumor cells were resuspended in 5 mL pre-warmed TSM medium. Tumor spheres were split every 5-7 days using Accutase (Invitrogen™) and single cells were reseeded. The concentration of growth factors was halved at every passage. After four passages, no growth factors were added to the TSM medium and cells were passaged two more times. Three cell lines from three independent *NES-Cre*$^{+}$*, LSL-PLAG1*$^{+}$*;Trp53*$^{fl/fl}$ tumors (1× female, 2× male) were generated and tested regularly for mycoplasma contamination (Mycoplasma PCR Kit, abm #G238). Expression of *PLAG1* in the growth factor depleted cells was validated via RNA sequencing and western blotting.

Western Blotting

Cells were resuspended in RIPA lysis buffer with protease and phosphatase inhibitors (Halt™ #78440) and protein concentration was assessed via BCA assay. For detection of PLAG1 in tumor spheroid cell lines, 25 ug of total protein was subjected to SDS PAGE on a 4%-12% gradient gel. Proteins were separated at 120 V for 2.5 h and transferred on a PVDF membrane using the iBlot™ 2 (Invitrogen). The membrane was blocked in 5% dry milk powder in TBST for 1h, and then the primary antibody was added in the same blocking solution (Cell signaling HA-Tag [C29F4] Rabbit mAb #3724 1:500, Proteintech PLAG1 polyclonal antibody #18018-1-AP 1:500, HRP-linked Anti-Actin antibody Loading Control #ab49900 1:10000). The membrane was rolled overnight at 4°C. The next day, the membrane was washed 3x in TBST, and the secondary antibody was added (Anti-rabbit IgG, HRP-linked Antibody [Cell Signaling #7074S] 1:2500 in blocking solution). After 1h incubation, the membrane was washed 2× in TBST and 1× in TBS. The chemiluminescent substrate (Cytiva ECL™ Prime #RPN2232) was added, and signal was detected using the Intas ECL Chemostar.

Lentiviral Transduction

Lentiviral expression plasmid (LentiCas9-Blast, Addgene #52962; pLenti-guide-mCherry, Addgene #185474) was transfected into HEK293T with the lentiviral packaging plasmids pMD2.G (VSV-G envelope, Addgene #12259) and psPAX2 (Addgene #12259) using FuGENE (Promega). Supernatant was collected every day for three days, filtered through a 0.45 µm PES membrane, and viral particles were concentrated using Lenti-X concentrator (Takara). Tumor spheroids were dissociated into single cells using Accutase (Invitrogen) and cells were seeded in a 12-well plate at a density of 2 million cells per mL. The lentiviral concentrate was added, and the cells were centrifuged at 930×*g* for 2 h at 30°C. The plate was incubated at 37°C and 5% CO_2 for 16 h. The next day, cells were washed twice with PBS and reseeded at a density of 200,000 cells per mL in ultra-low attachment flasks (Corning). After 24 h, selection was initiated by adding 2.5 µg/mL blasticidin to the medium. Cells were kept in culture for 7 days with replenishment of blastcidin when the medium was changed. Successful expression of Cas9 was validated via Western blotting.

DNA Extraction and Methylation-Array Based CNV Calculation

DNA was isolated from fresh frozen tissue or FFPE sections using the Maxwell RSC Tissue DNA Kit or the Maxwell RSC DNA FFPE Kit. 1200 ng DNA per sample was loaded on an Illumina MouseMethylation 285k or Illumina FFPE

MouseMethylation 285k chip and scanned according to manufacturer's protocols. CNVs from the methylation array data were analyzed using the R package conumee2 (v2.1)[27] with fresh-frozen, healthy Bl6N brain control DNA or FFPE-derived, Bl6N peritoneum DNA as controls.

Whole-Genome CRISPR Cas9 Screen

The protocol was adapted from Abid *et al.* 2023.[28] Briefly, *Cas9*-positive cells were infected with the mouse CRISPR brie virus library (Addgene #73633, clone pool CP0044) at an infection rate of 30% after selection for 2 days with 1.5 µg/mL puromycin. Two independent replicates per cell line were carried out. After selection, the Day-0 early timepoint cells were pelleted to obtain 50 million cells, corresponding to a guide representation of 500 cells/guide. Cells were then split in two chambers and individually passaged five times over a duration of 17 days with a guide representation of 500 cells/guide prior to sample collection of late time point (two technical replicates for each infection). DNA from both early and late time points was extracted using the Machery-Nagel Blood XL kit and sequenced according to previously published protocols.[29] Depleted genes were analyzed using the Broad Institute Genetic Perturbation Platform (GPP) pipeline Apron and the python package chronos.[30]

Single CRISPR-Cas9 Knockouts

sgRNA sequences were designed using CHOPCHOP[31] or taken from the CRISPR Brie library (Addgene #73633) and are depicted in Supplemental Table 3. After cloning into the pLenti-guide-mCherry vector (Addgene #185474), lentiviral particles were produced and Cas9-expressing cells were infected at an infection rate between 30%-50%. *Nras* and *PLAG1* guides were introduced in all three independent cell lines. *Reg4*, *Hsd3b2*, *Ngf*, *Spin2d* and *Mtr* guides were introduced in one cell line, which was not used for the whole genome CRISPR Cas9 screen. The proportion of mCherry-positive cells was assessed at different timepoints after selecting for live, single cells using a LSRFortessa flow cytometer (BD).

Results

The GFAP-Cre Lineage is Insufficient to Generate PLAG1*-Driven Brain Tumors*

As some of the CNS embryonal tumors with *PLAG* family gene alteration showed scattered or diffuse GFAP staining in the tumor and concurrent absence of other histopathological markers,[19,20] we chose the glial-lineage-specific *GFAP-Cre* driver line to express *PLAG1* in the developing mouse brain. Here, transgene activation should occur around embryonic day 13 (e13) in the dorsal medial telencephalon.[7] We crossed the *LSL-PLAG1* mouse line[14] to the *GFAP-Cre* driver line, with or without the addition of a floxed *Trp53* knock-out allele (Figure 1A). Unexpectedly, we observed that 60% of *GFAP-Cre*$^{+}$; *LSL-PLAG1*$^{+}$ mice developed abdominal tumors by 200 days, without the formation of brain tumors. Instead, mice frequently had reduced brain sizes (Figure S1A and B). Additional homozygous loss of *Trp53* increased penetrance and shortened latency, with 90% of the animals developing abdominal tumors by 100 days (Figure 1B). The tumor location varied around the lateroventral abdomen of the mice (Figure 1C). All tumors showed prominent PLAG1-HA staining and high KI67 staining by immunohistochemistry (IHC), indicating aggressive tumor growth (Figure 1D). *GFAP-Cre*$^{+}$; *Trp53*$^{fl/fl}$ control animals developed brain tumors by around 200 days (Figure S2). Intriguingly, in *GFAP-Cre*$^{+}$; *LSL-PLAG1*$^{+}$; *Trp53*$^{fl/fl}$ mice, no brain tumors formed prior to abdominal tumor onset, indicating that the *GFAP-Cre* lineage is insufficient for the purpose of modeling *PLAG1*-dependent brain tumors.

Nes-Cre *Mediated Overexpression of* PLAG1 *and Loss of* Trp53 *Leads to Embryonal-like Brain Tumors*

Nes-Cre-mediated transgene activation starts earlier than *GFAP-Cre* and is already detected at e10 in the neural tube.[32] A noticeable overlap in physiological transcript expression of *Nes* and *Plag1* is observed in the developing mouse brain at e11 (Figure 2A). Therefore, we next crossed the *LSL-PLAG1* line to a *Nes-Cre* driver line (Figure 2A). None of the *Nes-Cre*$^{+}$, *LSL-PLAG1*$^{+}$ mice developed tumors (Figure 2B). Instead, mice had reduced brain sizes and often showed signs of behavioral deficiencies (Figure S1C and D). No PLAG1-HA positive cells were detected in the brains (Figure S2E), indicating that expression in early cell types is either toxic or promotes dormancy, reducing their expansion and consequently leading to reduced brain size. With additional *Trp53* loss, however, 100% of *Nes-Cre*$^{+}$, *LSL-PLAG1*$^{+}$; *Trp53*$^{fl/fl}$ mice developed brain tumors by 100 days (Figure 2B). In contrast, only 50% of the control *Nes-Cre*$^{+}$, *Trp53*$^{fl/fl}$ animals developed brain tumors within the 1-year observation period, with a longer latency of 280 days on average (Figure 2B). *Nes-Cre*$^{+}$, *LSL-PLAG1*$^{+}$; *Trp53*$^{fl/fl}$ tumors presented in different brain regions, including both the forebrain and hindbrain, with a tendency towards ventral localization (Figure 2C). Control *Nes-Cre*$^{+}$, *Trp53*$^{fl/fl}$ tumors were only observed in the forebrain (Figure 2C). In H&E staining, *Nes-Cre*; *LSL-PLAG1*$^{+}$; *Trp53*$^{fl/fl}$ tumors exhibit poor differentiation, typically demonstrate high cellularity composed of small, round to oval cells with hyperchromatic nuclei and scant cytoplasm and lack distinct morphological organization (Figure 2D, S3A). The tumors were enriched for PLAG1-HA, the proliferation marker KI67, the early oligodendroglial-lineage marker OLIG2 and the stem cell marker SOX2, with more than 50% of nuclei stained positive (Figure 2D-F). Patchy staining for the glial lineage marker GFAP (around 40% positive area) and sparse SOX10 expression (around 20% positive nuclei) was observed (Figure 2D-F, S3B). With strong expression of the stem cell marker SOX2 and the undifferentiated appearance in the H&E staining, the model first appeared promising as it mostly recapitulated the embryonal-like, undifferentiated nature of human CNS embryonal tumors with PLAG family gene alteration.[19,20]

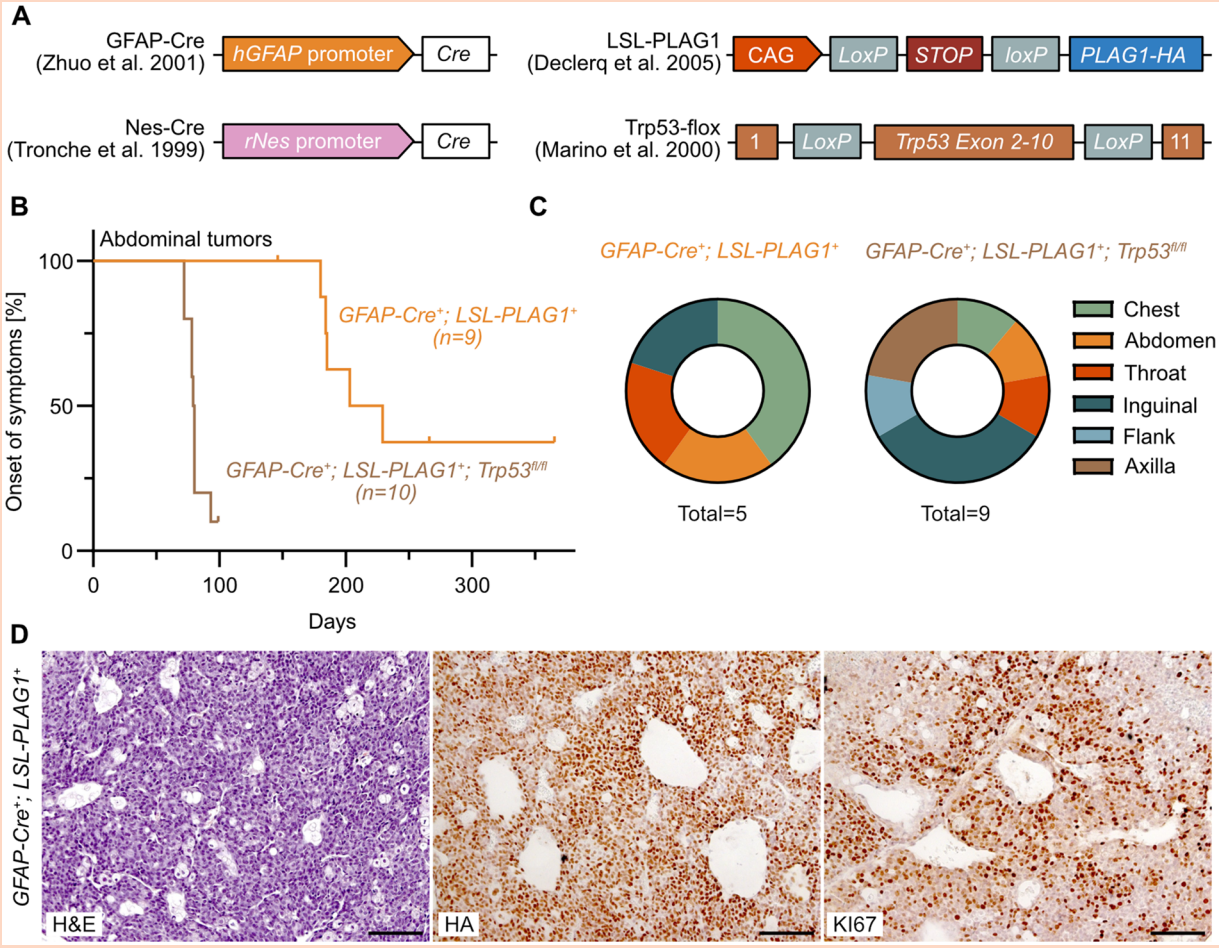

Figure 1. Overexpression of *PLAG1* in the *GFAP-Cre* lineage leads to the formation of abdominal tumors. (A) Schematic of transgene cassettes used and corresponding literature references. [Created in BioRender. Vaillant, J. (2025) https://BioRender.com/axmetyj]. (B) Kaplan-Meyer curves of transgenic mice depicting the time until endpoint criteria were met. (C) Location of abdominal tumors. (D) Hematoxylin and eosin (H&E) staining, anti-HA and anti-Ki67 IHC of example abdominal tumor sections. Scale bar, 100 µm.

Tumors Form with a Concurrent Gain/Loss at the Transgene Insertion Site on Chromosome 3

Murine tumor models can harbor recurrent CNVs beyond those directly targeted by the original genetic engineering strategy,[33] and *Trp53* inactivation is known to favor genomic instability.[34] As a rapid measure to assess the integrity of our newly generated models, we performed methylation-array based CNV analysis of tumor DNA (Figure 3A and B). All *Nes-Cre*$^{+}$; *LSL-PLAG1*$^{+}$; *Trp53*$^{fl/fl}$ tumors harbored a specific gain/loss pattern on chromosome 3 (Figure 3A). *GFAP-Cre*$^{+}$; LSL-*PLAG1*$^{+}$ abdominal tumors did not show this CNV (Figure S4), but we also detected this CNV pattern in the abdominal *GFAP-Cre*$^{+}$; LSL-*PLAG1*$^{+}$; *Trp53*$^{fl/fl}$ tumors (Figure 3B). To improve resolution, we performed whole-genome sequencing on *Nes-Cre*$^{+}$; *LSL-PLAG1*$^{+}$; *Trp53*$^{fl/fl}$ tumor DNA and matched tail DNA as control. In the control tissue, *Cre* is not expressed, so the LSL-cassette remains intact. We observed that the gain proceeds to the same nucleotide position in all tumors (example shown in Figure 3C). By displaying soft clipped reads, an integration event at this site in the tumor was visible (Figure 3C). The tails did not show this gain/loss, but instead displayed a second integration event (Figure 3C). Given that CNS tumors only formed in the presence of *Trp53* loss, we speculated that this copy number alteration would induce cell death in a *Trp53* wild-type context, rather than promote tumor formation. Taken together, Cre-mediated recombination of the *LSL-PLAG1* transgene leads to *PLAG1* overexpression and simultaneous copy number alterations at the target site (Figure 3D), introducing another layer of complexity into the model.

The Gained Chromosome 3 Region Substantially Affects Tumor Biology and Genetic Dependencies

Given that the generated brain tumors overexpressed *PLAG1* and also showed concurrent copy number gains on chromosome 3, we investigated the molecular

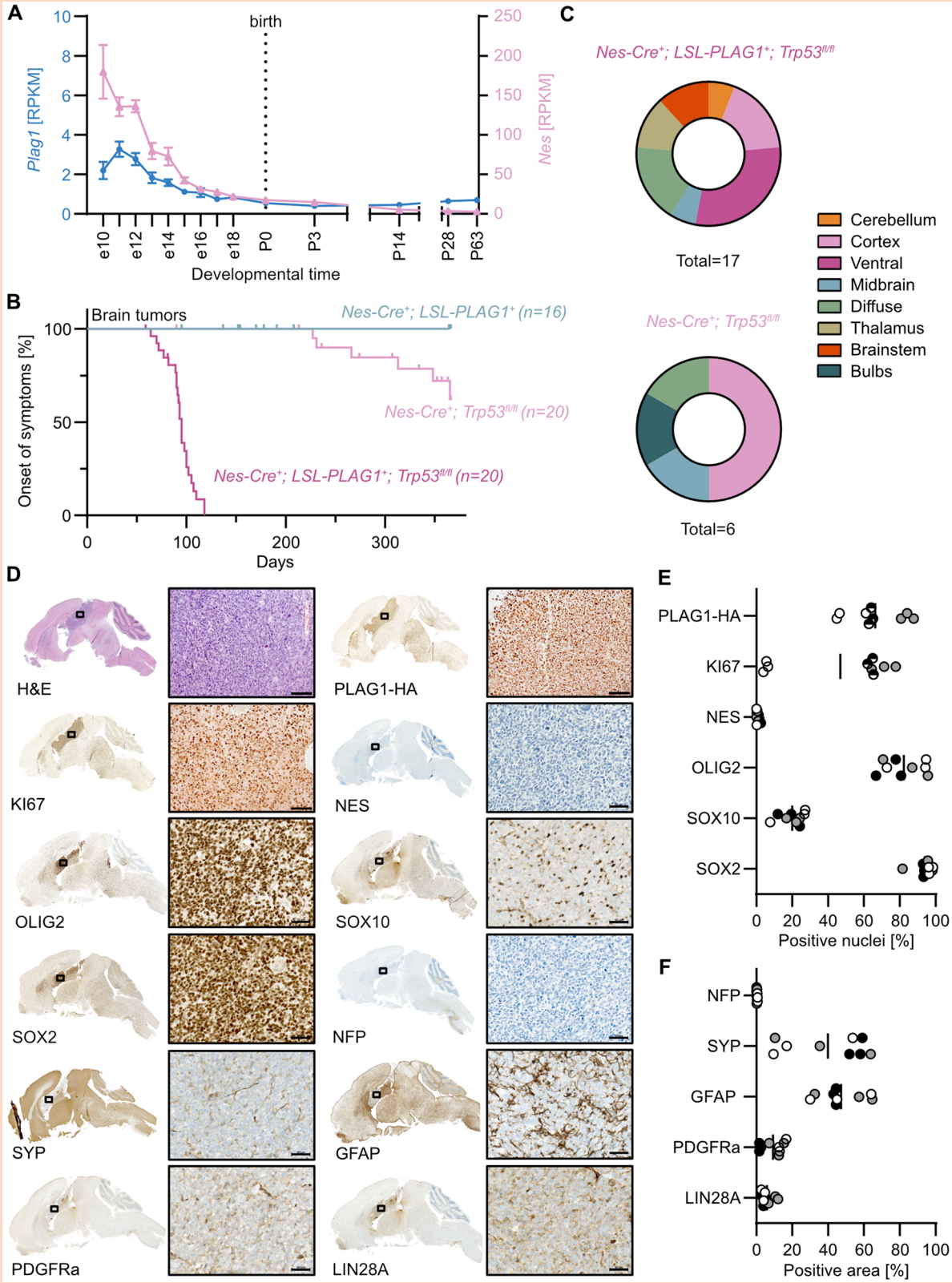

Figure 2. Overexpression of *PLAG1* with *Trp53* loss in the *Nes-Cre* lineage leads to the formation of embryonal-like tumors. (A) Reads Per Kilobase Million (RPKM) of *Nestin* and *Plag1* transcripts in the developing mouse brain. Error bars represent standard deviation. Data from Cardoso-Moreira *et al.* 2019. (B) Kaplan-Meyer curves of transgenic mice depicting the time until endpoint criteria were met. (C) Varying location of obtained brain tumors in transgenic mice. (D) Immunohistochemical detection of various marker proteins. H&E, HA, KI67 scale bar, 100 µm, NES, NFP, SYP, GFAP, OLIG2, PDGFRa, SOX10, LIN28A, SOX2 scale bar, 50 µm. (E) Quantification of nuclear markers in three 50×50 µm regions of interest in 3 tumors, representing by different dot colors. (F) Quantification of non-nuclear markers measured by area of positive stained regions.

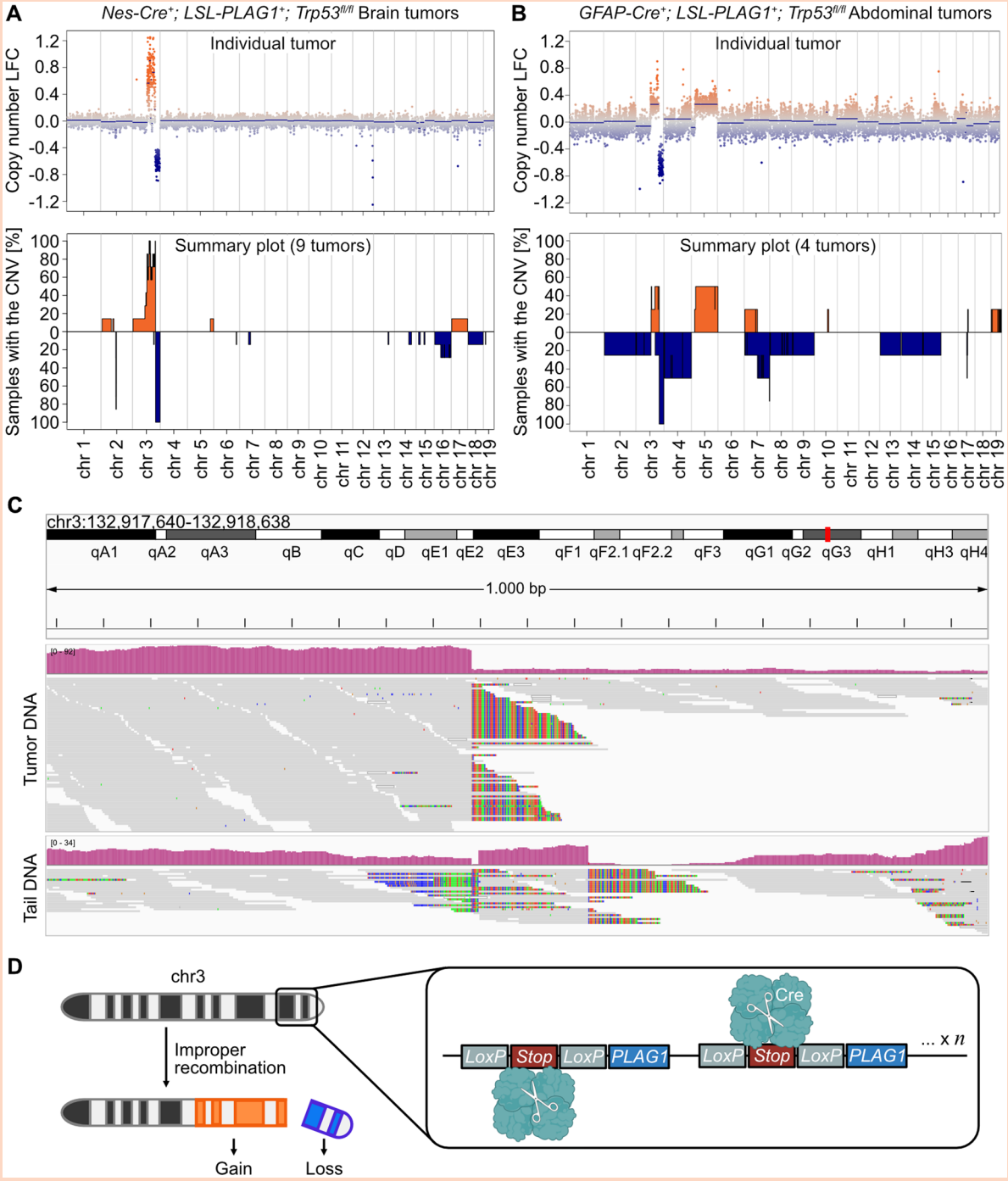

Figure 3. Methylation profiling identifies a copy-number alteratoin at the transgene insertion site. (A) CNV plot of one representative example (top) and summary plot of 9 *Nes-Cre*$^{+}$, *LSL-PLAG1*$^{+}$; *Trp53*$^{fl/fl}$ brain tumors (bottom) from fresh frozen samples. (B) CNV plot of one representative example (top) and summary plot of 4 different *GFAP-Cre*$^{+}$, *LSL-PLAG1*$^{+}$; *Trp53*$^{fl/fl}$ abdominal tumors (bottom) from FFPE samples. (C) Aligned reads of tumor DNA (upper panel) and tail DNA (lower panel). Soft clipped reads are depicted, with mismatched bases are colored. (D) Schematic of how the chromosome 3 CNV at the putative transgene insertion site could be generated. [Created in BioRender. Vaillant, J. (2025) https://BioRender.com/ccpz9fc].

consequences of these genetic changes to determine whether the model could still be reliably used to study the effects of *PLAG1* overexpression. Following bulk RNA-sequencing, we found that transcripts of known *PLAG1* and *PLAGL1* targets were upregulated, including *Cdkn1c, H19 and Dlk1.*[35-37] These genes are also upregulated in CNS embryonal tumors with *PLAGL1/2* amplification and *PLAG1* fusion.[19,20] The imprinted gene *Pappa2,* developmental genes of the HoxC cluster, and *Igf2bp1* were also upregulated (Figure 4A).

We also observed a large proportion of significantly upregulated genes located in the gained region on

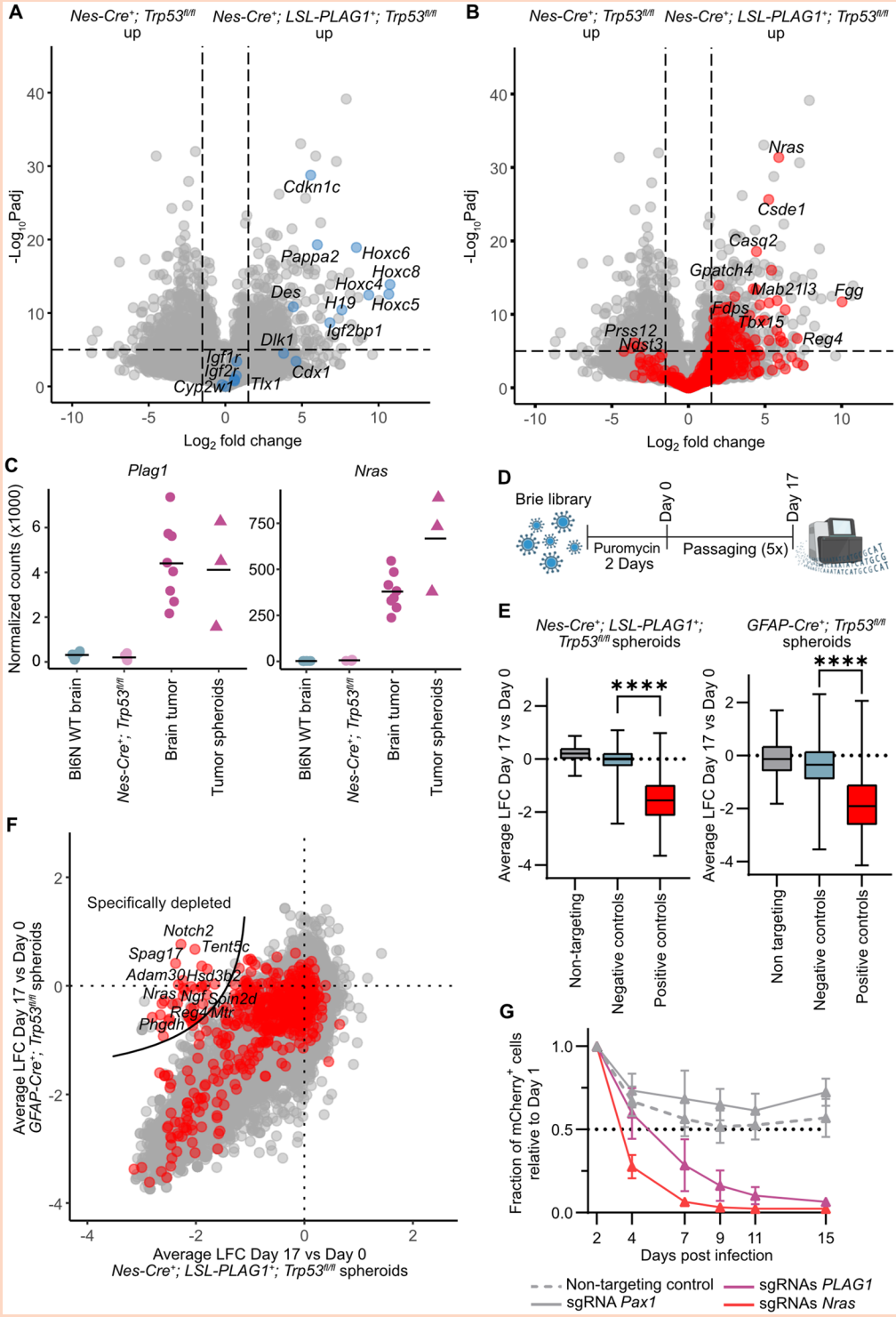

Figure 4. Genes in the amplified region shape the tumor transcriptome and genetic dependencies. (A) Differentially expressed genes in *NES-Cre*$^{+}$, *LSL-PLAG1*$^{+}$; *Trp53*$^{fl/fl}$ tumors ($n=9$) compared with *NES-Cre*$^{+}$; *Trp53*$^{fl/fl}$ control tumors ($n=5$). Known transcriptional targets and associated genes of *PLAG* family members labeled in blue. (B) Same comparison as in A, except genes located in the gained region on chromosome 3 shown in red. (C) Normalized counts of *Plag1* and *Nras* transcripts in *NES-Cre*$^{+}$, *Trp53*$^{fl/fl}$ control tumors, *NES-Cre*$^{+}$, *LSL-PLAG1*$^{+}$; *Trp53*$^{fl/fl}$ brain tumors, and spheroid cell lines derived from the latter. (D) Timeline of whole-genome CRISPR-Cas9 screen. [Created in BioRender. Vaillant, J. (2025) https://BioRender.com/vha2u33] (E) Average log fold changes (LFCs) of negative and positive control guides. Box represents the interquartile range with the median and whiskers indicate minimum and maximum values. Unpaired t-test, $P<0.0001$. (F) Average LFC for each gene (dots) in a *PLAG1*-positive spheroid cell line (x-axis) and a *PLAG1*-negative control cell line (*GFAP-Cre*$^{+}$; *Trp53*$^{fl/fl}$, y-axis) of 4 replicates each (for details see Methods). Red, genes located in the gained region on chromosome 3. (G) Three independent Cas9-positive tumor spheroids infected with mCherry labelled guides against *PLAG1* ($n=2$, black line), *Nras* ($n=2$, dotted line) or controls (non-targeting and *Pax1* targeting, grey line). Error bars indicate standard deviation.

chromosome 3 (Figure 4B). The most conspicuous upregulated gene was the MAPK regulator and proto-oncogene *Nras*, which was also expressed in spheroid cell lines derived from the tumors (Figure 4C). These growth factor-independent spheroid cell lines continued to express *PLAG1* (Figure 4C), including at the protein level (Figure S5). To identify genetic dependencies, we performed a whole-genome CRISPR-Cas9 knock-out screen (Figure 4D). Quality control measures showed depletion of universal dependency genes (positive controls) compared with negative controls targeting intergenic sites (Figure 4E). After 17 days *in vitro*, we observed a set of ~50 genes as specifically depleted in the *PLAG1*-positive cell line compared with the *PLAG1*-negative control cell line. Remarkably, most of the genes were located in the gained region of chromosome 3 (Figure 4F). As a higher number of gene copies can also lead to a higher number of Cas9-induced DNA breaks and corresponding DNA-damage induced stress, we corrected the screen hits for copy number changes using Chronos[30] (see Methods for details). We continued to observe amplified chromosome 3 genes as the top hits (Figure S6A and B). To validate *Nras* and other genes as true dependencies, we performed single CRISPR-Cas9 mediated knockout experiments in independent cell lines. Importantly, we observed that mCherry-labelled *PLAG1*- and *Nras* sgRNAs decreased cell proliferation in three independent cell lines, compared with control sgRNAs (Figure 4G), indicating that both genes are specific dependencies. Intriguingly, single KO experiments of other chromosome 3 genes *Reg4*, *Hsd3b2* and *Ngf* did not lead to a similar depletion, although the tested cell line harbored the same amplification (Figure 4D, S6C). While these genes could not be validated as model-specific dependencies, this data shows that targeting chromosome 3 itself does not affect tumor growth. Non-chromosome 3 genes *Spin2d* and *Mtr* were confirmed as dependencies in an independent cell line (Figure S6D), validating additional hits arising from the whole-genome CRISPR screen. Overall, the CNV we observed in our murine model has fundamental implications on shaping tumor dependencies, at least in modulating the effect that *PLAG1* overexpression has on tumor biology.

Discussion

Despite the frequent use of transgenic Cre-LoxP mouse models in research, unanticipated effects of the recombination can occur, so it is important to identify them accurately. We set out to generate a new transgenic mouse model for *PLAG1*-overexpressing pediatric brain tumors. The resulting model initially appeared promising, as tumor histology was similar to human patient samples, including an embryonal-like phenotype, and several upregulated genes were found to be in common with CNS embryonal tumors with *PLAG1* fusion or *PLAGL1/2* amplification (ET, PLAG).[19,20] We discovered, however, that our model contained a copy number alteration likely caused by improper Cre recombination of LoxP sites at the transgene insertion site. This alteration encompassed a 10 Mb region around the *Nras* locus with adjacent 23 Mb loss of the telomeric end of chromosome 3. Methylation array-based analysis was able to reliably detect this CNV. Furthermore, we showed that the genetic dependencies of the model are significantly shaped by this CNV, with most of the unique dependencies located in the gained region. Given its prevalence, we hypothesize that selective pressure might favor the CNV formation in a putative cell-of-origin, possibly by cooperating with initial *PLAG1* activation. While we observed the chromosome 3 gain both in brain tumors and abdominal tumors, only the brain tumors show high expression of *Nras*. Indeed, *PLAG1* was shown to regulate MAPK signaling via *IGF2* expression,[18] and IGF2 signaling regulates *NRAS* expression in hepatocellular carcinoma.[38] Therefore, we speculate that the *Nras* amplification we identified in our model might potentiate *PLAG1*-induced IGF2 signaling.

The *LSL-PLAG1* mouse strain used was generated via pronuclear injection of DNA fragments.[14] This process can lead to tandem integration at DNA break points, so called concatemers.[39] Repetitive or inverted LoxP sites could be one explanation for impaired Cre recombination, which in combination with *Trp53* loss could induce the large copy number alteration that we observed in the brain tumors. Abdominal tumors using *GFAP*-Cre driver lines also showed this copy number effect, but only with *Trp53* loss. Reduced brain sizes were observed crossing *LSL-PLAG1* mice to both *GFAP-Cre* and *Nes-Cre* driver lines with intact *Trp53*, so we speculate that the occurrence of the CNV triggers *Trp53*-mediated cell death, which could reduce the pool of neural progenitor cells and therefore reduce brain size. One obstacle of pronuclear injection is the random integration of transgenes. Therefore, recent methods to generate transgenic mice mostly rely on site specific insertion, for example in the *Rosa26* locus,[40] although some exceptions can be found.[41] Using such a safe-harbor integration site has the advantage of eliminating some uncertainties. However, we also identified examples in the literature that showed focal high-level amplifications at the *LSL-MYCN* transgene site within the *Rosa26* locus, using different Cre-driver lines.[42,43] Therefore, even with known transgene integration sites and especially with unknown integration sites, the analysis of global CNVs should be considered as a standard workflow when reporting novel transgenic models. Methylation array-based analysis has proven to be time- and cost-efficient. This method can identify possible copy number artifacts during early model characterization, ensuring that new findings can be safely translated into the next preclinical steps.

Supplementary Material

Supplementary material is available online at *Neuro-Oncology Advances* (https://academic.oup.com/noa).

Keywords

animal models | CNV | pediatric brain tumor | PLAG1 | preclinical model

Author Contributions

Conceptualization: LMK, DTWJ. Methodology: JV, LMK, SP. Formal analysis: JV, JM, MS, US, MKK, MZ. Investigation: JV, FS, PS, NH, AW, ABY, SP, PZ, TF. Writing - Original Draft: JV. Writing - Review & Editing: All authors. Visualization: JV. Supervision: LMK, DTWJ, RB, PB. Funding acquisition: LMK, DTWJ, RB, PB.

Conflict of Interest Statement

None declared.

Funding

This work was funded by the The Brain Tumour Charity Quest for Cures Consortium Grant GN-000691 to RB, PB, DTW, and LMK. US was supported by the Fördergemeinschaft Kinderkrebszentrum Hamburg. JV was supported by the German Cancer Aid Short Term Fellowship Program (#70115681).

Acknowledgments

We thank Wim J.M. Van de Ven and KU Leuven for kindly sharing the *LSL-PLAG1* mouse strain. We acknowledge the Broad Institute Genetic Perturbation Platform for the CRISPR Brie virus library production and assistance in data analysis. We thank the following core facilities at the DKFZ: Next Generation Sequencing, Microarray, Microscopy, Flow Cytometry, and Center for Preclinical Research (CPR). Figure 1A, Figure 3D and Figure 4D were created with Biorender.

Ethics Approval

All animal experiments for this study were conducted according to the animal welfare regulations approved by the responsible authorities (Regierungspraesidium Karlsruhe, approval number: G-35/20).

Data Availability

Raw data will be made available upon reasonable request.

Affiliations

Developmental Origins of Pediatric Cancer Junior Research Group, German Cancer Research Center (DKFZ), Germany (J.V., P.Z., F.S., T.F., L.M.K.); Division of Pediatric Glioma Research, German Cancer Research Center (DKFZ), Heidelberg, Germany (J.V., A.W., A.B.-Y., M.-K.K., D.T.W.J.); National Center for Tumor Diseases (NCT), NCT Heidelberg, a partnership between DKFZ and Heidelberg University Hospital, German (J.V., J.M., A.W., A.B.-Y., P.Z., F.S., N.H., M.-K.K., M.Z., D.T.W.J., L.M.K.); Hopp Children's Cancer Center Heidelberg (KiTZ), Heidelberg, Germany (J.V., J.M., A.W., A.B.-Y., P.Z., F.S., N.H., M.-K.K., T.F., M.Z., D.T.W.J., L.M.K.); Faculty of Biosciences, Heidelberg University, Heidelberg, Germany (J.V.); Department of Medical Oncology, Dana-Farber Cancer Institute, Boston (S.P., R.B.); Department of Pediatric Oncology, Dana-Farber/Boston Children's Cancer and Blood Disorders Center, Boston (S.P., P.B.); Harvard Medical School, Boston (S.P., R.B., P.B.); Broad Institute of MIT and Harvard, Cambridge (S.P., R.B., P.B.); Department of Pediatric Hematology and Oncology, University Medical Center Hamburg-Eppendorf, Germany (M.S., U.S.); Research Institute Children's Cancer Center Hamburg, Germany (M.S., U.S.); Mildred Scheel Cancer Career Center HaTriCS4, University Medical Center Hamburg-Eppendorf, Hamburg, Germany (M.S.); Institute of Neuropathology, University Medical Center Hamburg-Eppendorf, Germany (U.S.); Division of Pediatric Neurooncology, German Cancer Research Center (DKFZ), Heidelberg, Germany (F.S., N.H., M.Z.); Department of Neuropathology, Institute of Pathology, University Hospital Heidelberg, Heidelberg, Germany (P.S.); Clinical Cooperation Unit Neuropathology, German Consortium for Translational Cancer Research (DKTK), German Cancer Research Center (DKFZ), Heidelberg, Germany (P.S.)

References

1. Tam PPL, Ho JWK. Cellular diversity and lineage trajectory: insights from mouse single cell transcriptomes. *Development*. 2020;147:dev179788.
2. Budhu S, Wolchok J, Merghoub T. The importance of animal models in tumor immunity and immunotherapy. *Curr Opin Genet Dev*. 2014;24:46-51.
3. Cheon D-J, Orsulic S. Mouse models of cancer. *Annu Rev Pathol*. 2011;6:95-119.
4. Petrescu DI, Yustein JT, Dasgupta A. Preclinical models for the study of pediatric solid tumors: focus on bone sarcomas. *Front Oncol*. 2024;14:1388484.
5. Kersten K, de Visser KE, van Miltenburg MH, Jonkers J. Genetically engineered mouse models in oncology research and cancer medicine. *EMBO Mol Med*. 2017;9:137-153.
6. Sternberg N, Hamilton D. Bacteriophage P1 site-specific recombination. I. Recombination between loxP sites. *J Mol Biol*. 1981;150:467-486.
7. Zhuo L, Theis M, Alvarez-Maya I, Brenner M, Willecke K, Messing A. hGFAP-cre transgenic mice for manipulation of glial and neuronal function in vivo. *Genesis*. 2001;31:85-94.
8. Tronche F, Kellendonk C, Kretz O, et al. Disruption of the glucocorticoid receptor gene in the nervous system results in reduced anxiety. *Nat Genet*. 1999;23:99-103.
9. Filbin M, Monje M. Developmental origins and emerging therapeutic opportunities for childhood cancer. *Nat Med*. 2019;25:367-376.
10. Loonstra A, Vooijs M, Beverloo HB, et al. Growth inhibition and DNA damage induced by cre recombinase in mammalian cells. *Proc Natl Acad Sci U S A*. 2001;98:9209-9214.
11. Harno E, Cottrell EC, White A. Metabolic pitfalls of CNS *Cre*-Based technology. *Cell Metab*. 2013;18:21-28.
12. Song AJ, Palmiter RD. Detecting and avoiding problems when using the cre/lox system. *Trends Genet*. 2018;34:333-340.

13. Kas K, Voz ML, Röijer E, et al. Promoter swapping between the genes for a novel zinc finger protein and β-catenin in pleiomorphic adenomas with t(3; 8)(p21; q12) translocations. *Nat Genet*. 1997;15:170-174.
14. Declercq J, Van Dyck F, Braem CV, et al. Salivary gland tumors in transgenic mice with targeted PLAG1 proto-oncogene overexpression. *Cancer Res*. 2005;65:4544-4553.
15. Arias-Stella JA, Benayed R, Oliva E, et al. Novel PLAG1 gene rearrangement distinguishes a subset of uterine myxoid leiomyosarcoma from other uterine myxoid mesenchymal tumors. *Am J Surg Pathol*. 2019;43:382-388.
16. Santisukwongchote S, Thorner PS, Desudchit T, et al. Pediatric fibromyxoid tumor with fusion: an emerging entity with a novel intracranial location. *Neuropathology*. 2022;42:315-322.
17. Fritchie K, Wang L, Yin Z, et al. Lipoblastomas presenting in older children and adults: analysis of 22 cases with identification of novel *PLAG1* fusion partners. *Mod Pathol*. 2021;34:584-591.
18. Zheng Y, Xu L, Hassan M, et al. Bayesian modeling identifies PLAG1 as a key regulator of proliferation and survival in rhabdomyosarcoma cells. *Mol Cancer Res*. 2020;18:364-374.
19. Keck M-K, Al-Hussaini M, Amayiri N, et al. PLAG1 fusions define a third subtype of CNS embryonal tumor with PLAG family gene alteration. *Acta Neuropathol*. 2025;150:12.
20. Keck M-K, Sill M, Wittmann A, et al. Amplification of the PLAG-family genes-PLAGL1 and PLAGL2-is a key feature of the novel tumor type CNS embryonal tumor with PLAGL amplification. *Acta Neuropathol*. 2023;145:49-69.
21. Sievers P, Henneken SC, Blume C, et al. Recurrent fusions in PLAGL1 define a distinct subset of pediatric-type supratentorial neuroepithelial tumors. *Acta Neuropathol*. 2021;142:827-839.
22. Jenseit A, Camgöz A, Pfister SM, Kool M. EZHIP: a new piece of the puzzle towards understanding pediatric posterior fossa ependymoma. *Acta Neuropathol*. 2022;143:1-13.
23. Cardoso-Moreira M, Halbert J, Valloton D, et al. Gene expression across mammalian organ development. *Nature*. 2019;571:505-509.
24. Marino S, Vooijs M, van Der Gulden H, Jonkers J, Berns A. Induction of medulloblastomas in p53-null mutant mice by somatic inactivation of Rb in the external granular layer cells of the cerebellum. *Genes Dev*. 2000;14:994-1004.
25. Love MI, Huber W, Anders S. Moderated estimation of fold change and dispersion for RNA-seq data with DESeq2. *Genome Biol*. 2014;15:550.
26. Zhu A, Ibrahim JG, Love MI. Heavy-tailed prior distributions for sequence count data: removing the noise and preserving large differences. *Bioinformatics*. 2019;35:2084-2092.
27. Daenekas B, Pérez E, Boniolo F, et al. Conumee 2.0: enhanced copy-number variation analysis from DNA methylation arrays for humans and mice. *Bioinformatics*. 2024;40:btae029.
28. Abid T, Goodale AB, Kalani Z, et al. Genome-wide pooled CRISPR screening in neurospheres. *Nat Protoc*. 2023;18:2014-2031.
29. Piccioni F, Younger ST, Root DE. Pooled lentiviral-delivery genetic screens. *Curr Protoc Mol Biol*. 2018;121:32.1.1-32.1.21.
30. Dempster JM, Boyle I, Vazquez F, et al. Chronos: a cell population dynamics model of CRISPR experiments that improves inference of gene fitness effects. *Genome Biol*. 2021;22:343.
31. Labun K, Montague TG, Krause M, Torres Cleuren YN, Tjeldnes H, Valen E. CHOPCHOP v3: expanding the CRISPR web toolbox beyond genome editing. *Nucleic Acids Res*. 2019;47:W171-W174.
32. Graus-Porta D, Blaess S, Senften M, et al. β1-class integrins regulate the development of laminae and folia in the cerebral and cerebellar cortex. *Neuron*. 2001;31:367-379.
33. Schoof M, Zheng T, Sill M, et al. Investigation of a global mouse methylome atlas reveals subtype-specific copy number alterations in pediatric cancer models. *Nat Genet*. 2026;58:143-156.
34. Fukasawa K, Wiener F, Woude GFV, Mai S. Genomic instability and apoptosis are frequent in p53 deficient young mice. *Oncogene*. 1997;15:1295-1302.
35. Keyvani Chahi A, Belew MS, Xu J, et al. PLAG1 dampens protein synthesis to promote human hematopoietic stem cell self-renewal. *Blood*. 2022;140:992-1008.
36. Voz ML, Mathys J, Hensen K, et al. Microarray screening for target genes of the proto-oncogene PLAG1. *Oncogene*. 2004;23:179-191.
37. Varrault A, Gueydan C, Delalbre A, et al. Zac1 regulates an imprinted gene network critically involved in the control of embryonic growth. *Dev Cell*. 2006;11:711-722.
38. Ji Y, Wang Z, Li Z, et al. Silencing IGF-II impairs C-myc and N-ras expressions of SMMC-7721 cells via suppressing FAK/PI3K/akt signaling pathway. *Cytokine*. 2017;90:44-53.
39. Smirnov A, Battulin N. Concatenation of transgenic DNA: random or orchestrated? *Genes (Basel)*. 2021;12:1969.
40. Nyabi O, Naessens M, Haigh K, et al. Efficient mouse transgenesis using gateway-compatible ROSA26 locus targeting vectors and F1 hybrid ES cells. *Nucleic Acids Res*. 2009;37:e55.
41. Zhu X, Chen J, Wang B, et al. A mouse model for high-efficient flp-recombinase-mediated genetic manipulation in the pancreas. *Pancreatology*. 2023;23:736-741.
42. Schoof M, Godbole S, Albert TK, et al. Mouse models of pediatric high-grade gliomas with MYCN amplification reveal intratumoral heterogeneity and lineage signatures. *Nat Commun*. 2023;14:7717.
43. Althoff K, Beckers A, Bell E, et al. A cre-conditional MYCN-driven neuroblastoma mouse model as an improved tool for preclinical studies. *Oncogene*. 2015;34:3357-3368.